Optical terminal analysis of a multigrating tiled compressor in a PW-class CPA-laser*

Yang Yu-Chuan(杨雨川)[a)b)†], Luo Hui(罗 晖)[a)], Wang Xiao(王 逍)[b)], Li Fu-Quan(李富全)[b)], Huang Xiao-Jun(黄小军)[b)], and Jing Feng(景 峰)[b)]

[a)] College of Optoelectric Science and Engineering, National University of Defense Technology, Changsha 410073, China
[b)] Research Center of Laser Fusion, China Academy of Engineering Physics, Mianyang 621900, China

(Received 6 April 2011; revised manuscript received 5 July 2011)

In the highest-power chirped-pulse amplification lasers, the pulse must be stretched in time, amplified, compressed in a grating compressor and subsequently focused by off-axis parabola to obtain a high peak power. In the optical terminal, the temporal and spatial effects of mismatched multigrating tiled compressor on the far-field pulse are critical factors to be analysed. In this paper, a ***k***-space raytracing model is proposed for the temporal and spatial analyses of possible errors in a four-grating single-pass tiled compressor. The results show that the last grating affects mainly the partial focal spot, while the middle two gratings affect the temporal waveform, and the partial focal spot needs much higher error control than that in the temporal domain in a picosecond pulse compression.

Keywords: high-power chirped-pulse amplification lasers, optical terminal, multigrating tiled compressor, off-axis parabola

PACS: 42.65.Re, 42.79.Dj **DOI:** 10.1088/1674-1056/21/1/014210

1. Introduction

The development of ultra-short lasers based on chirped-pulse amplification (CPA) makes it possible to realize ultrahigh intensity laser systems with focused intensities up to about 10^{24} W/cm^2 in extreme light infrastructure (ELI). To amplify a short high-power laser pulse, it must be stretched firstly because otherwise it may cause damage to the optics required for amplifying it. After being stretched through time, the pulse must be recompressed and focused by an off-axis parabola to the target.[1−3] To do this, an optical terminal should be designed to satisfy the targeting requirement and forecast the targeting results. A multigrating compressor is required, which will allow for a stretched pulse to be propagated through it. When going through the compressor, the pulse is separated by wavelength before being focused together. Since the diffraction gratings required by the pulse compressors need to be quite large, the array gratings are placed in series to form each complete diffraction grating.

Qiao *et al.*[4] have analysed the single tiled tolerance on partial distribution in OMEGA EP (extended performance) compressor consisted of four tiled gratings. Harimoto[5] has analysed the far-field pattern for a single 2×2 tiled grating. For FIREX (fast ignition realization experiment), a diamond-type tiled compressor is applied, and the PETAL (petawatt aquitaine laser) compressor scheme is based on coherent addition of beams instead of coherent addition of gratings.[6,7] In these complicated multigrating tiled compressors, a general model should be built to analyse the temporal and spatial properties of the targeting pulse after it passing through the compressor and the off-axis parabolic mirror. A similar active phase adjustment has also been applied to the two-dimensional phase array grating.[8] In this paper, we use a ***k***-space raytracing model to analyse the temporal and spatial properties of the targeting pulse, and study the effects of misalignments on the focusing in a 4-grating single-pass tiled compressor for chirped pulse laser.

2. Temporal and spatial algorithm

If the irradiance profiles of arbitrary light propagating along the z direction in free space are represented by the matrix $\boldsymbol{A}(x, y)$, any well-behaved function may be written as a summation of spatial fre-

*Project supported by the National High Technology Research and Development Program of China (Grant No. 2009AA8044005).
†Corresponding author. E-mail: yyc_online@126.com
© 2012 Chinese Physical Society and IOP Publishing Ltd

quency components as

$$\boldsymbol{A}(x,y) = \int_{-\infty}^{\infty}\int_{-\infty}^{\infty} \boldsymbol{A}(\xi,\eta) \times \exp(2\pi\jmath(x\xi+y\eta))\mathrm{d}\xi\,\mathrm{d}\eta, \quad (1)$$

where $\boldsymbol{A}(\xi,\eta)$ is a two-dimensional (2D)-Fourier transform (FT) of $\boldsymbol{A}(x,\ y)$. A plane wave in $\boldsymbol{k}$-notation is propagated by

$$\boldsymbol{A}(\boldsymbol{k},z) = \boldsymbol{A}(\boldsymbol{k},0)\cdot\exp(\jmath\boldsymbol{k}z). \quad (2)$$

The variation of the phase factors $\exp(\jmath\boldsymbol{k}z)$ depends on the propagation distance z and the $\boldsymbol{k}$-vector, so the phase aberration related to deviation can be expressed by[9]

$$\begin{aligned}\Delta\Phi(x,y,z) &= \Delta\boldsymbol{k}\cdot[x,\ y,\ z]^{\mathrm{T}} \\ &= \Delta k_x x + \Delta k_y y + \Delta k_z z, \end{aligned} \quad (3)$$

where $\Delta\boldsymbol{k} = (\Delta k_x,\ \Delta k_y,\ \Delta k_z)$. According to Fraunhofer diffraction, the far-field diffraction pattern for wave propagating in the homogeneous media along $\boldsymbol{k}$-vector is

$$\boldsymbol{A}(X,Y,\Delta\Phi) \propto \mathrm{FT}\{\exp(\jmath\Delta\Phi)\boldsymbol{A}(x,y,0)\}. \quad (4)$$

The corresponding calculation for pulse compression with the grating compressor can be also carried out by means of the 2D-FT. We assume the unity amplitude incident laser pulse on the compressor to be

$$E(t) = \exp[-(1-\jmath b)t^2/T^2 - \jmath\omega_0 t], \quad (5)$$

where b is quadratic phase chirp and T is the input pulse duration. Reference [10] gives the output of the grating compressor in the frequency domain as

$$E(\omega) = \left(\frac{\pi}{1-\jmath b}\right)^{1/2} T\exp\left\{-\frac{(\omega-\omega_0)^2T^2}{4(1-\jmath b)}\right\} \times \exp[\jmath\Delta\Phi(\omega)], \quad (6)$$

where $\Delta\Phi(\omega)$ corresponds to the phase shift for an arbitrary wavelength λ up to the phase front at λ_0. By the inverse 2D-FT of Eq. (5), the compressed pulse in time domain is obtained.

3. $\boldsymbol{k}$-space raytracing

In order to apply the propagation formalism introduced in Eq. (3), the direction of propagation z has to be defined for each ray segment and wavelength, respectively. Appropriate coordinate systems must be chosen for each segment. Multiple rays have to be traced simultaneously, namely a reference and several tilted rays.

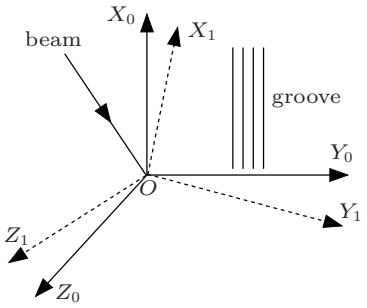


Fig. 1. Illustration of the standard and error grating system.

In Fig. 1, the reference grating coordinate system $X_0Y_0Z_0$ is assumed to be perfectly aligned with respect to the first grating, and the deviation grating coordinate system $X_1Y_1Z_1$ is aligned with respect to the deviation grating.[9,11] Assuming the incident wave vector is $\boldsymbol{k}_{\mathrm{in}} = (k_{\mathrm{i}\,x}, k_{\mathrm{i}\,y}, k_{iz})$, according to the grating equation,

$$(\boldsymbol{k}_{\mathrm{in}} - \boldsymbol{k}_{\mathrm{out}}) \times N = \left[\frac{m\lambda}{d}G, 0, 0\right]^{\mathrm{T}}. \quad (7)$$

Here, d is the grating space, λ is the incident laser wavelength, and $\boldsymbol{k}_{\mathrm{out}}$ is the exciting wave vector, which can be written as

$$\boldsymbol{k}_{\mathrm{out}} = \left[\frac{m\lambda}{d} - k_{\mathrm{i}\,x}, k_{\mathrm{i}\,y}, \sqrt{1-\left(\frac{m\lambda}{d}-k_{\mathrm{i}\,x}\right)^2 - k_{\mathrm{i}\,y}^2}\right]^{\mathrm{T}}, \quad (8)$$

where m is the grating diffraction order and T represents the transpose of a matrix. The rotations around the x-axis, y-axis and z-axis are respectively described as α_x, α_y, α_z, and that of the corresponding transposed matrixes are $\boldsymbol{R}_x$, $\boldsymbol{R}_y$, $\boldsymbol{R}_z$.

$$\begin{aligned}\boldsymbol{R}_x &= \begin{bmatrix} 1 & 0 & 0 \\ 0 & \cos\alpha_x & -\sin\alpha_x \\ 0 & \sin\alpha_x & \cos\alpha_x \end{bmatrix}, \\ \boldsymbol{R}_y &= \begin{bmatrix} \cos\alpha_y & 0 & \sin\alpha_y \\ 0 & 1 & 0 \\ -\sin\alpha_y & 0 & \cos\alpha_y \end{bmatrix}, \\ \boldsymbol{R}_z &= \begin{bmatrix} \cos\alpha_z & -\sin\alpha_z & 0 \\ \sin\alpha_z & \cos\alpha_z & 0 \\ 0 & 0 & 1 \end{bmatrix}. \end{aligned} \quad (9)$$

In consideration of the tilted angle, the exciting wave vector is given by $\boldsymbol{R}_{x,y,z}$ and $\boldsymbol{k}_{\mathrm{in}}$. Applying grat-

ing Eq. (4), the exiting wave vector should be transformed to $X_0Y_0Z_0$ by left multiplication transpose of matrix $\boldsymbol{R}_{x,y,z}$ as

$$\boldsymbol{k}'_{\text{out}} = \boldsymbol{k}_{\text{in}} + \boldsymbol{R}^{-1}_{x,y,z} \times \frac{m\lambda}{d} G. \tag{10}$$

For the off-axis parabola, the paraboloid of revolution equation is

$$x^2 + y^2 = 4fz, \tag{11}$$

where f is the focal length. Assuming the crossing point between the incident beam and the paraboloid of revolution is $(x_0,\ y_0,\ z_0)$, the normal vector at the crossing point is $\boldsymbol{k}_{\text{normal}} = (x_0/f,\ y_0/f,\ -1)$, so the exiting wave vector $\boldsymbol{k}''_{\text{out}}$ corresponding to the incident wave vector $\boldsymbol{k}'_{\text{in}}$ is calculate by $\boldsymbol{k}''_{\text{out}} = \boldsymbol{k}'_{\text{in}} + \boldsymbol{k}_{\text{normal}}$.

4. Numerical simulation

We take a 4-grating single-pass tiled compressor as a calculation example, which is shown in Fig. 2 for picosecond (ps) compression used in fast ignition research.[12] In this multi-grating tiled compressor, the global coordinate system (GCS) is different from the local coordinate system (LCS) linked to the grating surface. The related typical parameters about the optical terminal are as follows: the Groove intensity is 1740 mm^{-1}, the incident angle is 71°, the center distances are 2.4 and 5.8 m, the grating gap is 5 mm, the tiled grating size is 910 mm×300 mm, the the focal length f of the parabolic mirror is 800 mm, the off-axis angle is 45°, and the beam size is 285 mm×285 mm.

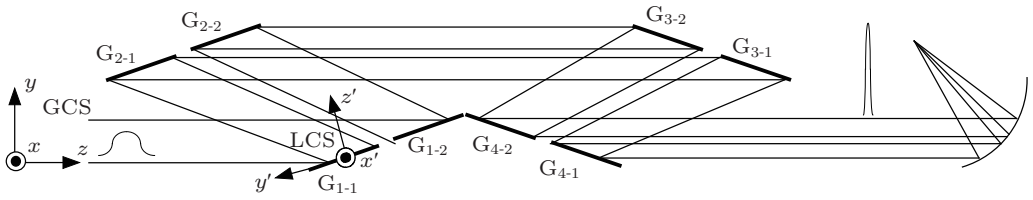


Fig. 2. Section plane of the 4-grating single-pass tiled compressor and off-axis parabolic mirror.

The incident chirped pulse in the spatial domain is

$$\boldsymbol{A}(x,y,0) = \exp\left\{-\left[\left(\frac{x}{R}\right)^{2n} + \left(\frac{y}{R}\right)^{2n}\right]\right\} \times \exp(-\mathrm{J}\phi_0(x,y)), \tag{12}$$

where $\Phi_0(x,y)$ is the initial wavefront phase, R is the waist of super-Gauss laser beam and n is the super-Gauss order. The related typical parameters about the incident beam are chosen as $R = 100$ mm and $n = 10$.

4.1. Results in spatial domain

The phase difference calculated by z and $\boldsymbol{k}$-vector related to the far-field irradiance is computed for four degrees of freedom (the α_x, α_y, α_z are described in the LCS and Δz is described in the GCS) and incident static wavefront aberration Φ_0. The phase map $\Delta\Phi(x,y)$ numerically defined by $N\times N$ matrix is composed of an $N \times N/2$ zero matrix (diffracted by the subgrating $G_{1\text{-}1}$) concatenated with an $N \times N$ matrix (diffracted by the subgrating $G_{1\text{-}2}$). The far-field diffraction patterns of grating $G_{1\text{-}1}$ rotation of respectively α_x, α_y, α_z = 1, 2, 3 μrad and Δz = 66.3 nm, 132.5 nm, 265 nm are shown in Fig. 3. Figure 4 shows the evolution of Strehl ratio for various amounts of angle errors in the case of a perfectly flat incoming wavefront.

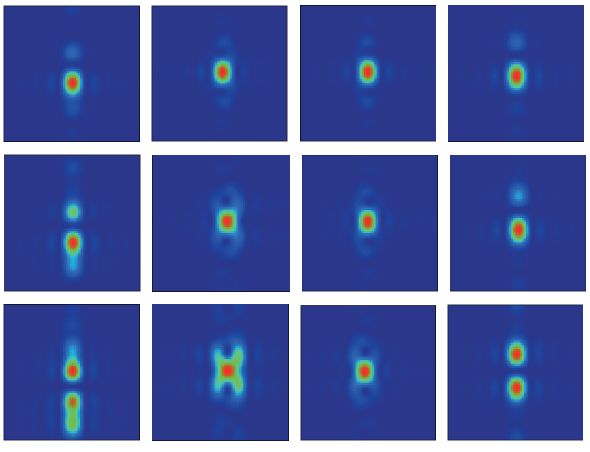


Fig. 3. (colour online) Representation of far-field intensity distribution with differential angles (the image size is 32 μm×32 μm). The upper panels, α_x, α_y, α_z = 1 μrad, Δz = 66.3 nm; the middle panels, α_x, α_y, α_z = 2 μrad, Δz = 132.5 nm; the lower panels, α_x, α_y, α_z = 3 μrad, Δz = 265 nm.

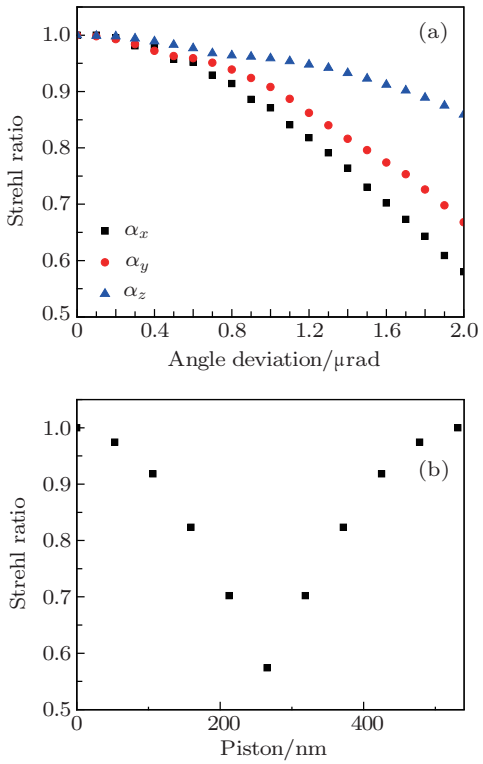


Fig. 4. (colour online) Strehl ratio sensitivity analysis to α_x, α_y, α_z (a) and Δz (b) misalignment.

The α_x, α_y, α_z rotation of grating $G_{1\text{-}1}$ and Δz phase default tolerances to have a peak intensity reduction less than 10% correspond to $\alpha_x = 0.87$ μrad, $\alpha_y = 1.05$ μrad, $\alpha_z = 1.7$ μrad, and $\Delta z = 120$ nm respectively. According to the calculation process, the α_x, α_y, α_z rotation of $G_{2\text{-}1}$, $G_{3\text{-}1}$ and $G_{4\text{-}1}$ to have a peak intensity reduction less than 10% are listed in Table 1. In Eq. (11), the initial phase $\Phi_0(x, y)$ is fitted with rectangle Zernike polynomial to analyse the distorted wavefront effect. The wavefront distortion tolerances to have a peak intensity reduction $< 10\%$ correspond to wavefront PV (peak to valley) < 0.7 and RMS(root-mean-square) < 0.09. In the partial domain, the last tiled grating requires the highest precision.

Table 1. The tolerances to a peak intensity reduction of 10% (unit: μrad).

	$G_{1\text{-}1}$	$G_{1\text{-}2}$	$G_{1\text{-}3}$	$G_{1\text{-}4}$
α_x	0.87	0.87	0.87	0.64
α_y	1.05	0.94	1.05	0.94
α_z	1.7	1.55	1.7	1.55

4.2. Results in temporal domain

The spectral phase with respect to the angular frequency is usually developed into a Taylor series in order to parametrize phase dispersion[13−15]

$$\phi'(\omega) = \phi'_0 + \phi'_1(\omega - \omega_0) + \phi'_2(\omega - \omega_0)^2 + \sum_n \phi'_n. \quad (13)$$

The first term of Eq. (12) takes into account of the absolute phase of the electromagnetic field, which is generally not measurable. The second term describes a spatial pulse shift. The temporal pulse profile is not changed by the Φ'_1 term, while the $\Phi'_2, \ldots, \Phi'_n$ terms induce a temporal distortion of the pulse. A raytracing is carried out for the aligned grating compressor model. The dispersion curve is shown in Fig. 5 and the fitting polynomial is

$$\phi'(\omega) = 5.87996 \times 10^9 - 6.26052 \times 10^{-6}(\omega - \omega_0) + 1.69411 \times 10^{-21}(\omega - \omega_0)^2. \quad (14)$$

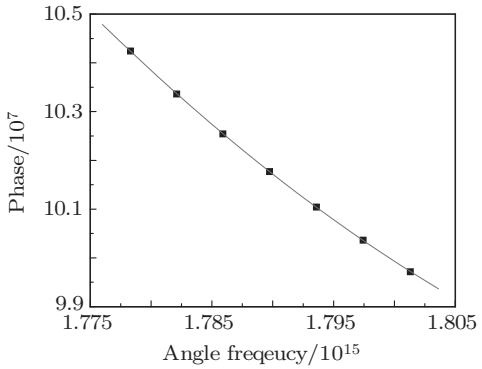


Fig. 5. Aligned grating compressor dispersion curve based on the example given in Fig. 2.

According to Ref. [16], the ideal compression condition is $bT^2/(1 + b^2) = 4\Phi'_2$, where Φ'_2 is the dispersion coefficient. Assuming the quadratic phase shift is -466, when the input chirped pulse has a temporal duration of $T = 1.8$ ns, the compression pulse duration is 6.35 ps (the half-height full width in Eq. (4)). In the high-energy PW laser system for fast ignition, the typical temporal duration is 10 ps.[17,18] When the high-order dispersion is completely compensated, the temporal expression of chirped pulse after compression is

$$E(t) \propto \exp(\mathrm{J}(\phi_0 - \omega_0 t)) \exp(-(t - \phi_1)^2/T_0^2). \quad (15)$$

When the high-order dispersion is not compensated, the inverse Fourier transform of Eq. (5) is used to analyse the high-order dispersion effect. The real curves in Fig. 6 show the result considering high-order dispersion, and the signal-to-noise ratio is $10^{10.48}$.

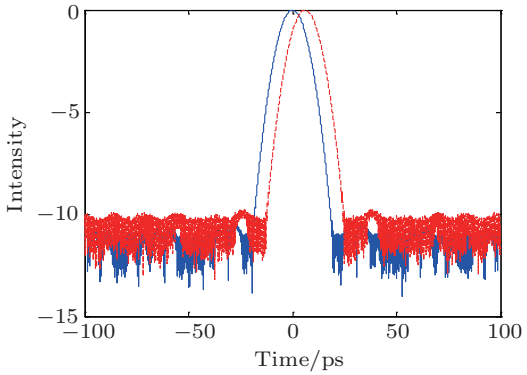


Fig. 6. (colour online) Effect of dispersion on the compressed pulse (logarithmic coordinates are used).

Under the condition of $G_{2\text{-}2}$ rotation $\alpha_x = 1$ mrad, the raytracing is carried out and the fitting polynomial is

$$\phi''(\omega) = 5.87739 \times 10^{9} - 6.25773\text{E} \times 10^{-6}(\omega - \omega_0) + 1.69335 \times 10^{-21}(\omega - \omega_0)^2. \quad (16)$$

The dashed curve in Fig. 6 presents the compression result after the misaligned compressor. In this figure, a tilt $\alpha_x = 1$ mrad induces a pulse desynchronization of 6 ps, the signal-to-noise ratio is less than $10^{9.78}$, and the pulse duration is broaden to 80 fs; a tilt $\alpha_y = 100$ μrad induces a pulse desynchronization of 0.2 ps with less effect on the pulse duration and signal-noise ratio; a tilt $\alpha_z = 1$ mrad induces a pulse desynchronization of 0.3 ps which can hardly affect the pulse duration and signal-to-noise ratio. In the symmetrical compressor layout, the tilt α_x rotation of $G_{3\text{-}2}$ has the same result as that of $G_{2\text{-}2}$ on the pulse group delay, and the tilt α_y rotation of $G_{4\text{-}2}$ has the same result as that of $G_{2\text{-}2}$ on the pulse group delay. The rotations of $G_{1\text{-}1}$ and $G_{1\text{-}4}$ have little effect on the temporal waveform up to the milliradian level misalignment. Therefore, in the symmetrical grating tiled compressor system, the rotation angles around the grating rules of G_2 and G_3 are the main parameters to decide the output pulse temporal waveform.

5. Experiments

To verity the calculation results, a testbed consisting of a single-pass two-grating tiled compressor is set up, which is shown in Fig. 7. The pulse laser with the center wavelength $\lambda_0 = 1053$ nm is injected from optical window W1, then goes through the grating compressor consisted of G1 and G2. The mirror M3 is a beam splitter, one beam is directed to the target and the other one is collimated and focused by the telescope system consisted of convexes L2 and L3. The G2 is a medium aperture tiled grating, and the grating is driven by high-precision stepping motor, achieving 60 nm/step after subdivision. Here, the circular input beam diameter is 100 mm (not a rectangle beam), and the other parameters are the same as those given in Section 4. Combining with the calculation model, we only consider the two front gratings in Fig. 2. Under the condition of having the same angle and piston misalignment, the far-field CCD captured and the simulated results are both shown in Fig. 8, proving a good agreement. We think the differences between them are mainly caused by wavefront distortion, actuator precision and beam vibration.

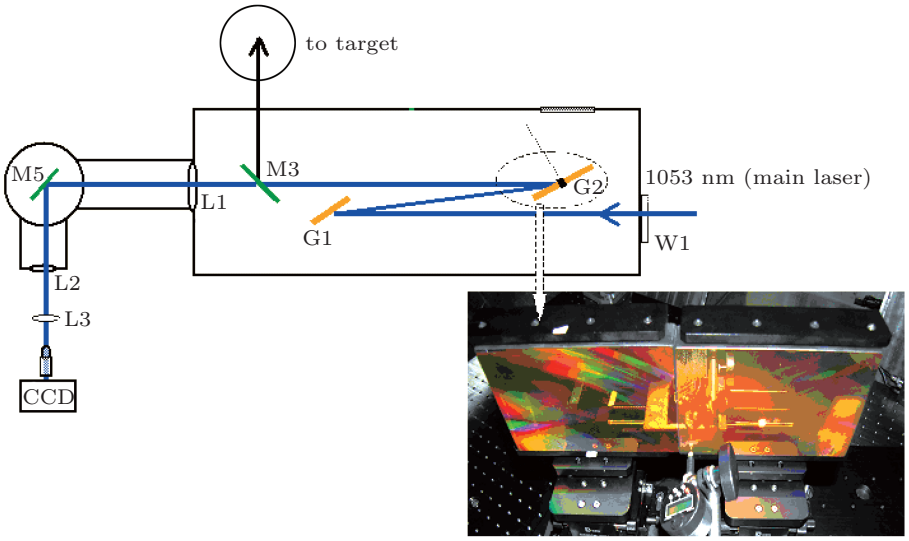
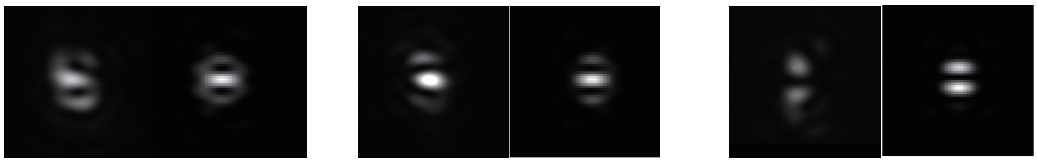


Fig. 7. (colour online) Optical schematic of grating compressor and tiled grating entity.



(a) (b) (c)

Fig. 8. The CCD captured images and simulated results: (a) $\alpha_y = 6$ μrad, (b) $\alpha_z = 6$ μrad, (c) piston=250 nm.

6. Conclusion

In conclusion, a raytracing model based on the $\boldsymbol{k}$-vector is built to analyse the partial and temporal properties of the multi-grating tiled compressor. In the four-grating tiled compressor, the last grating has the highest angle precision requirement of 0.64 μrad, 0.94 μrad and 1.55 μrad for good partial focal spot. However, in the temporal domain, the middle two gratings are the key parameters affecting the pulse desynchronization, pulse broaden and signal-to-noise ratio. Finally, the simulation results in the partial domain have been proven by the simplified testbed. With the development of high-power PW laser system, more and more compressors layout have been proposed, such as a diamond structure and a self-compensation structure.[3,15] The method proposed in this paper easily deals with these cases.

References

[1] Waxer L J, Maywar D N, Kelly J H, Kessler T J, Kruschwitz B E, Loucks S J, Mccrory R L, Meyerhofer D D, Morse S F B, Stoeckl C and Zuegel J D 2005 *Opt. Photonics News* **16** 30

[2] Blanc C L, Felix C, Lagron J C, Forget N, Hollander P, Sautivet A M, Sauteret C, Amiranoff F and Migus A 2003 *IFSA* X-608

[3] Habara H, Xu G and Jitsuno T 2010 *Opt. Lett.* **35** 1783

[4] Qiao J, Kalb A, Guardalben M J, King G, Canning D and Kelly J H 2007 *Opt. Express* **15** 9562

[5] Harimoto T 2004 *Jpn. J. Appl. Phys.* **43A** 1362

[6] Rushford M C, Britten J A, Barty C P J, Jitsuno T, Kondo K, Miyanaga N, Tanaka K A, Kodama R and Xu G 2008 *Opt. Lett.* **33** 1902

[7] Blanchot N, Bar E, Behar G, Bellet C, Bigourd D, Boubault F, Chappuis C, Coïc H, Damiens-Dupont C, Flour O, Hartmann O, Hilsz L, Hugonnot E, Lavastre E, Luce J, Mazataud E, Neauport J, Noailles S, Remy B, Sautarel F, Sautet M and Rouyer C 2010 *Opt. Express* **18** 10088

[8] Zhou B, Chen Y L, Li Y A and Li H W 2010 *Acta Phys. Sin.* **59** 1816 (in Chinese)

[9] Ma X M and Zhang W P 2009 *Journal of Guangxi University* **34** 858

[10] Zhang T J, Yonemura M and Kato Y 1998 *Opt. Commun.* **145** 367

[11] Hornung M, Bodefeld R, Siebold M, Podleska S, Schnepp M, Hein J and Sauerbrey R 2005 *Proc. SPIE* **5962** 59622k-1

[12] Zeng X H and Fan D Y 2010 *Acta Phys. Sin.* **59** 6312 (in Chinese)

[13] Fiorini C, Sauteret C, Rouyer C, Blanchot N, Seznec S and Migus A 1994 *IEEE J. Quantum Electron.* **30** 1662

[14] Fittinghoff D N, Walker B C, Squier J A, Toth C S, Rosepetruck C and Barty C P J 1998 *IEEE J. Select. Topics Quantum Electron.* **4** 430

[15] Li B C, Theobald W and Welsch E 2000 *Appl. Phys.* B **71** 819

[16] Treacy E 1969 *IEEE J. Quantum Electron.* QE25 454

[17] Miyanaga N, Azechi H, Tanaka K, Kanabe T, Jitsuno T, Kawanaka J, Fujimoto Y, Kodama R, Shiraga H, Knodo K, Tsubakimoto K, Habara H, Lu J, Xu G, Morio N, Matsuo S, Miyaji E, Kawakami Y, Izawa Y and Mima K 2006 *J. Phys. IV France* **133** 81

[18] Laboratory for Laser Energetics 2006 S-AD-M-005